Bioorganic Chemistry 81 (2018) 211–221

Contents lists available at ScienceDirect

Bioorganic Chemistry

journal homepage: www.elsevier.com/locate/bioorg

Searching for improved mimetic peptides inhibitors preventing conformational transition of amyloid-β_{42} monomer

János Gera[a], Titanilla Szögi[a], Zsolt Bozsó[a], Livia Fülöp[a], Exequiel E. Barrera[b], Ana M. Rodriguez[c,d], Luciana Méndez[e], Carina M.L. Delpiccolo[e], Ernesto G. Mata[e], Federica Cioffi[f], Kerensa Broersen[f], Gabor Paragi[a,g], Ricardo D. Enriz[c,d,*]

[a] Department of Medicinal Chemistry, University of Szeged, Dom ter 8, 6720 Szeged, Hungary
[b] Biomolecular Simulations Group, Institut Pasteur de Montevideo, Mataojo 2020, 11400 Montevideo, Uruguay
[c] Facultad de Química, Bioquímica y Farmacia, Universidad Nacional de San Luis, Chacabuco 915, 5700 San Luis, Argentina
[d] IMIBIO-SL (CONICET), Chacabuco 915, 5700 San Luis, Argentina
[e] Instituto de Química Rosario (CONICET-UNR), Facultad de Ciencias Bioquímicas y Farmacéuticas, Universidad Nacional de Rosario, Suipacha 531, 2000 Rosario, Argentina
[f] Nanobiophysics, Faculty of Science and Technology (TNW), Technical Medical Centre, University of Twente, The Netherlands
[g] MTA-SZTE Biomimetic Systems Research Group, Dom ter 8, 6720 Szeged, Hungary

ARTICLE INFO

Keywords:
Mimetic peptides
Alzheimer's disease
Amyloid β-peptide
Aβ aggregation
Molecular dynamics
Molecular docking

ABSTRACT

A series of novel mimetic peptides were designed, synthesised and biologically evaluated as inhibitors of $A\beta_{42}$ aggregation. One of the synthesised peptidic compounds, termed compound **7** modulated $A\beta_{42}$ aggregation as demonstrated by thioflavin T fluorescence, acting also as an inhibitor of the cytotoxicity exerted by $A\beta_{42}$ aggregates. The early stage interaction between compound **7** and the $A\beta_{42}$ monomer was investigated by replica exchange molecular dynamics (REMD) simulations and docking studies. Our theoretical results revealed that compound **7** can elongate the helical conformation state of an early stage $A\beta_{42}$ monomer and it helps preventing the formation of β-sheet structures by interacting with key residues in the central hydrophobic cluster (CHC). This strategy where early "on-pathway" events are monitored by small molecules will help the development of new therapeutic strategies for Alzheimer's disease.

1. Introduction

Alzheimer's disease (AD) is a complex, progressive, and irreversible neurological disorder being the most prevalent neurodegenerative disease in humans [1]. By 2030, the number of people with the disease is expected to rise to more than 70 million cases worldwide [2,3]. Unless there is a breakthrough in treatment, nearly one in every 2–3 people over 85 years of age will attain AD.

Although there are some controversies [4], the most widely accepted theory regarding the aetiology of AD is known as the "amyloid hypothesis" which features the amyloid β-peptide (Aβ) as the central pathological agent. This hypothesis posits that pathology initiates because of an imbalance in Aβ production and/or clearance, which may result from altered expression or processing of amyloid precursor protein (APP) or changes in Aβ metabolism [5]. Various forms of Aβ arise upon processing of APP, including peptides varying in length from 37 ($A\beta_{37}$) to 46 ($A\beta_{46}$) amino acids. It is widely accepted that the more amyloidogenic $A\beta_{42}$ is most dominantly toxic and accumulates in the brain of patients with AD [6].

In the last fifteen years, growing number of evidences suggest that the small oligomeric aggregates of Aβ, rather than the fibrillar products are the most cytotoxic species in neurodegenerative diseases [7,8]. Thus, strategies to prevent or destabilize the formation of Aβ aggregates by interfering with Aβ oligomers, particularly those related to $A\beta_{42}$ are workable approaches in the field of drug discovery against AD. Such approaches may include the blockage of protein–protein interactions that generate toxic Aβ aggregates [9] or the inhibition of conformational transition between the native disordered conformation of Aβ and the aggregation-prone β-sheet structures [10,11]. Insight into conformational transformation that trigger misfolding and amyloid formation is useful in the design of compounds that target these transitions [12,13]. Broad range of anti-Aβ aggregation agents, peptidic and non-peptidic inhibitors [14–16] nanoparticles [17], small molecules [18–20] have been designed recently to target protein misfolding.

* Corresponding author at: Facultad de Química, Bioquímica y Farmacia, Universidad Nacional de San Luis, Chacabuco 915, 5700 San Luis, Argentina.
E-mail address: denriz@unsl.edu.ar (R.D. Enriz).

https://doi.org/10.1016/j.bioorg.2018.08.018
Received 12 June 2018; Received in revised form 10 August 2018; Accepted 13 August 2018
Available online 18 August 2018
0045-2068/

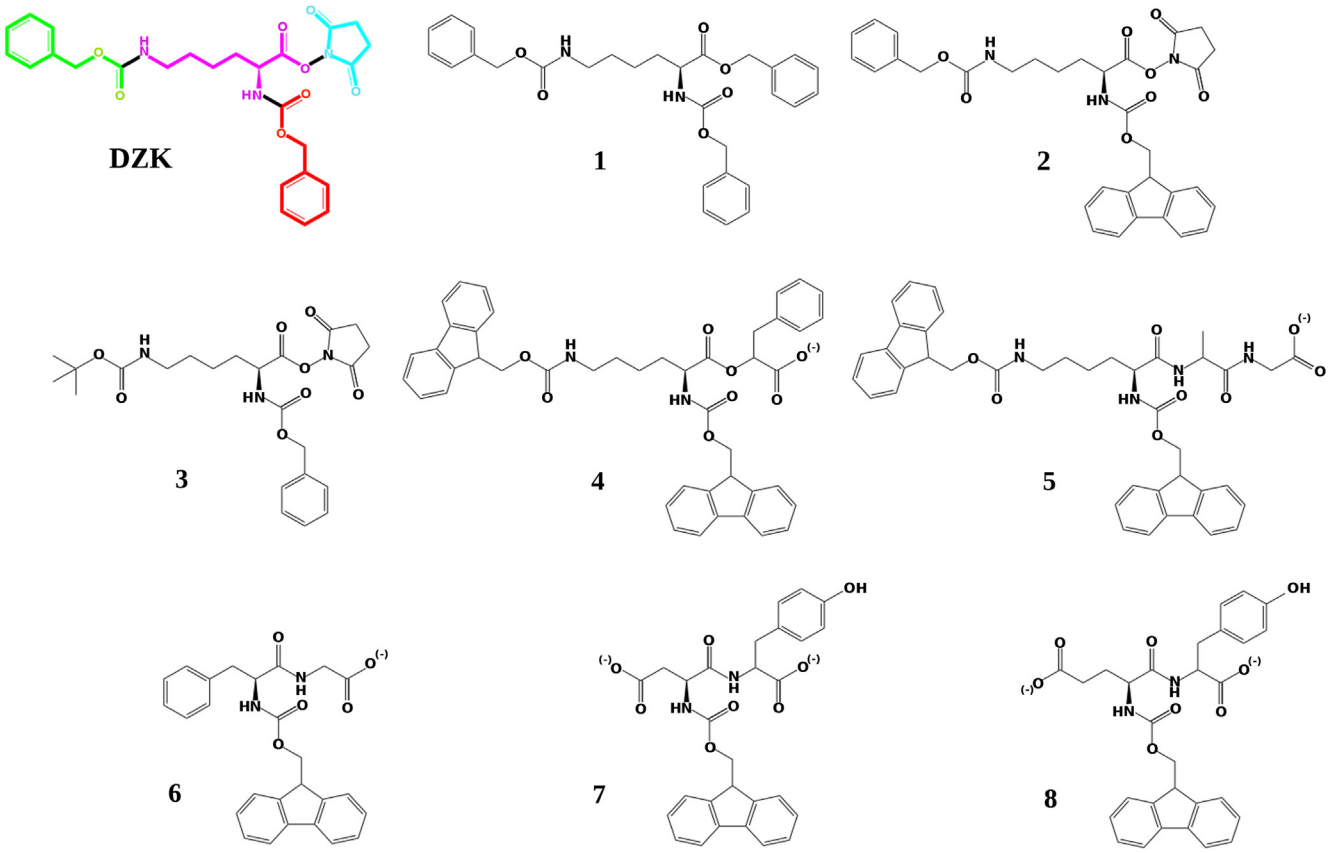

Fig. 1. DZK structure (core: in magenta, R1: in blue, R2: in red, *R*3: in green). Structure features of compounds **1–8.**

In order to design new molecules that prevent $A\beta_{42}$ aggregation more effectively, the detailed underlying molecular mechanism of inhibition of $A\beta_{42}$ aggregation should be elucidated. Despite the significant progress in methodologies, experiments can give a limited picture about the effect of small molecules in the early stage of the aggregation. Computational simulations, especially molecular dynamics (MD) can provide atomic level description of conformational transitions involved in peptide–ligand interactions. Recently, a large number of computational studies have been reported to elucidate the fundamental molecular mechanism of unfolding of the native conformation of $A\beta_{42}$ and to characterize the inhibition mechanisms of current Aβ inhibitors at atomic level [20].

In the search for new anti-aggregation agents, we have reported a series of mimetic peptides with potent inhibitory activity against the formation of $A\beta_{42}$ aggregates [21,22]. These compounds were derived from a molecular modelling study using as molecular target a pentameric Aβ model previously developed by our research group [23]. Among these compounds, **DZK** (*Nα*,*Nε*-Di-Z-L-lysine hydroxysuccinimide ester, Fig. 1) presented the most potent inhibiting properties, therefore in the present work this compound was taken as the starting structure in the search of new inhibitors.

Recently, we performed a theoretical study on **DZK** using QM/MM calculations and QTAIM analysis using an $A\beta_{42}$ monomeric model [24].

Following this work, we aimed to find new peptide-like structures that have an inhibitory effect against the formation of $A\beta_{42}$ aggregates based on combined theoretical-experimental study. In a first step, taking compound **DZK** as a starting point, we designed and synthesised several structurally related mimetic peptides. In the second stage, the anti-aggregation properties of these new compounds were evaluated by spectroscopy and microscopy techniques, while their capacity to inhibit $A\beta_{42}$-induced toxicity was monitored in an *in vitro* viability assay. To have insights of the atomic level interaction between the active compound and the monomeric $A\beta_{42}$ peptide a molecular modelling study was performed. This stage included docking calculations and enhanced sampling MD simulations.

2. Materials and methods

2.1. Chemistry

2.1.1. Synthesis

The strategy employed for the synthesis of dipeptides (**4, 6–8**) and

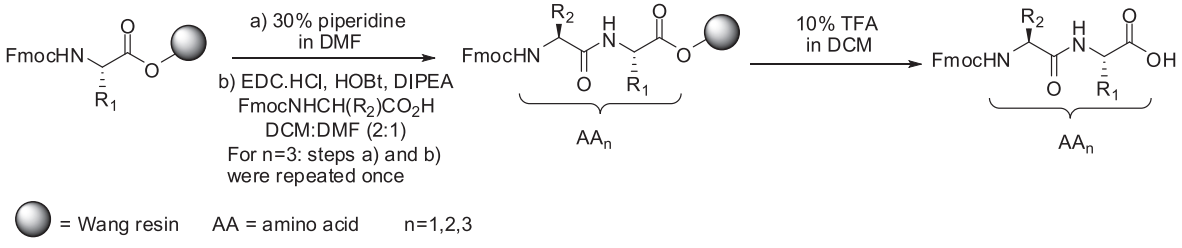

Scheme 1.

tripeptide (**5**) started with the Fmoc-protected amino acids preloaded to Wang resin which were treated with 30% piperidine in DMF to free the amino group (Scheme 1). The second or third amino acids were coupled using standard solid-phase peptide synthesis conditions, hydroxybenzotriazole (HOBt) and 1-ethyl-3-(3-dimethylaminopropyl)carbodiimide (EDC) [25,26]. The obtained immobilized peptides were cleaved from the solid support by treatment with 10% trifluoroacetic acid in dichloromethane.

Formation of *N*-hydroxysuccinimide esters **2** and **3** were carried out using standard conditions (*N*,*N*′-dicyclohexylcarbodiimide, *N*-hydroxysuccinimide). On the other hand, a lysine derivative of **1** was obtained by treatment of H-Lys(Z)OBn hydrochloride with benzyl chloroformate in the presence of triethylamine and 4-*N*,*N*-dimethylaminopyridine.

2.1.2. General

Chemical reagents were purchased from commercial sources and used without further purification. Solvents were analytical grade or were purified by standard procedures prior to use. ^{1}H NMR spectra were recorded on a Bruker Avance 300 spectrophotometer operating at 300 MHz. ^{13}C NMR spectra were recorded on the same apparatus at 75 MHz. Mass spectra were obtained on a LC-MS Bruker micrOTOF-Q II spectrophotometer. Silica gel aluminium plates (Merck 60 F254) were used for analytical TLC. Flash column chromatography was performed using Merck silica gel 60 (230–400 mesh).

2.1.3. General procedure I. Solid phase coupling

The Fmoc-amino acid-Wang resin (300 mg) was suspended in a 30% piperidine solution in DMF and stirred 50 min at r.t (room temperature). The resin was washed with CH_2Cl_2 (3 × 2 mL), EtOAc (3 × 2 mL), MeOH (3 × 2 mL) and CH_2Cl_2 (2 mL), and finally dried in vacuum. The resin was suspended in 5 mL of a DMF:DCM (2:1) mixture and Fmoc-amino acid (3 equiv.), 1-hydroxybenzotriazole (3 equiv.), 1-ethyl-3-(3-dimethylaminopropyl)carbodiimide (3 equiv.) and diisopropylethylamine (3 equiv.) were successively added. The solution was stirred at r.t. for 16 h. After this, the resin was washed with DMF (3 × 2 mL), CH_2Cl_2 (3 × 2 mL), MeOH (3 × 2 mL) and CH_2Cl_2 (2 mL), and finally dried in vacuum. Resin was treated with 5 mL of 10% TFA in CH_2Cl_2 for 1 h. The mixture was filtered and the filtrate was evaporated under reduced pressure to give the crude product.

2.1.4. General procedure II. Formation of N-hydroxysuccinimide ester

The amino acid was dissolved in CH_2Cl_2 and *N*-hydroxysuccinimide (1.2 equiv.) was added. The solution was cooled to 0 °C and *N*,*N*′-dicyclohexylcarbodiimide (1.2 equiv.) dissolved in CH_2Cl_2 was added dropwise. The mixture was stirred overnight at r.t., filtered, and the filtrate was evaporated under reduced pressure to give the crude product.

2.1.5. Z-Lys(Z)-OBn (1)

H-Lys(Z)OBn hydrochloride (100 mg, 0.24 mmol) was dissolved in anhydrous *N*,*N*-dimethylformamide, trimethylamine (50 μL, 0.36 mmol, 1.5 equiv.), benzyl chloroformate (51 μL, 0.36 mmol, 1.5 equiv.) and 4-dimethylaminopyridine (cat.) were successively added. The reaction mixture was stirred at 60 °C overnight. Purification by silica gel column chromatography (Hexane/EtOAc) gives 48 mg of product **1** (40% yield).

^{1}H NMR ($CDCl_3$, 300 MHz): δ (ppm) 7.35–7.28 (m, 15H), 5.17 (dd, J_1 = 17.8 Hz, J_2 = 12 Hz, 2H), 5.05 (m, 2H), 3.96 (m, 2H), 3.58 (t, J = 6.1 Hz, 1H), 3.06 (m, 2H), 1.87 (m, 2H), 1.36–1.19 (m, 4H). ^{13}C NMR ($CDCl_3$, 75 MHz): δ (ppm) 169.6, 156.5, 136.6, 134.6, 131.7, 129.9, 129.1, 128.9, 128.8, 128.7, 128.4, 128.0, 67.8, 66.5, 58.6, 50.2, 40.2, 29.8, 29.1, 21.9. HRMS calcd. for $C_{29}H_{32}N_2NaO_6^+$ ($[M + Na]^+$, *m/z*): 527.21526, found: 527.21473.

2.1.6. Fmoc-Lys(Z)-OSu (2)

Starting from Fmoc-Lys(Z)-OH (114 mg, 0.22 mmol) and following general procedure II, we obtained the crude material that was purified by silica gel column chromatography (Hexane/EtOAc), providing 72.3 mg of product **2** (55% yield).

^{1}H NMR ($CDCl_3$, 300 MHz): δ (ppm) 7.75 (d, J = 7.3 Hz, 2H), 7.58 (d, J = 7.3 Hz, 2H), 7.38–7.25 (m, 9H), 5.57 (m, 1H), 5.08 (s, 2H), 5.05 (m, 1H), 4.73 (m, 1H), 4.43 (m, 2H), 4.22 (m, 1H), 3.21 (m, 2H), 2.76 (s, 4H), 1.97–1.90 (m, 2H), 1.51 (m, 4H). ^{13}C NMR ($CDCl_3$, 75 MHz): δ (ppm) 168.6, 168.2, 156.6, 155.6, 143.8, 143.6, 141.3, 136.6, 128.4, 128.0, 127.7, 127.1, 125.0, 119.9, 67.2, 66.6, 52.1, 47.1, 40.2, 31.8, 29.1, 25.5, 21.6. HRMS calcd. for $C_{33}H_{33}N_3NaO_8^+$ ($[M + Na]^+$, *m/z*): 622.21599; found: 622.21553.

2.1.7. Z-Lys(Boc)-OSu (3)

Starting from (Z)-Lys(Boc)dicyclohexylamonium salt and following general procedure II, we obtained the crude material that was purified by silica gel column chromatography (Hexane/EtOAc), providing 75 mg of product **3** (98% yield).

^{1}HNMR ($CDCl_3$, 300 MHz): δ (ppm) 7.34 (m, 5H), 5.55 (m, 1H), 5.12 (s, 2H), 4.70 (m, 2H), 3.10 (m, 2H), 2.82 (s, 4H), 2.03–1.86 (m, 2H), 1.50 (m, 4H), 1.40 (s, 9H). ^{13}CNMR ($CDCl_3$, 75 MHz): δ (ppm) 168.6, 168.2, 156.2, 155.6, 135.9, 128.5, 128.2, 79.1, 67.3, 52.2, 39.6, 31.8, 29.4, 28.4, 25.5, 21.7. HRMS calcd. for $C_{23}H_{31}N_3NaO_8^+$ ($[M + Na]^+$, *m/z*): 500.20034, found: 500.19978.

2.1.8. Fmoc-Lys(Fmoc)-Phe-OH (4)

Starting from Fmoc-Phe-Wang resin (300 mg, 0.21 mmol, sust: 0.7 mmol/g) and following general procedure I, using Fmoc-Lys(Fmoc)-OH (372.1 mg, 0.63 mmol), we obtained the crude material that was purified by silica gel column chromatography (CH_2Cl_2/MeOH, 95:5, drops of AcOH) providing 96.9 mg of compound **4** (65% yield).

^{1}H NMR ($(CD_3)_2SO$, 300 MHz): δ (ppm) 8.05 (d, J = 8.1 Hz, 1H), 7.88–7.85 (m, 4H), 7.70–7.65 (m, 4H), 7.41–7.14 (m, 13H), 4.46–4.38 (m, 1H), 4.28–4.15 (m, 6H), 4.00–3.93 (m, 1H), 3.16 (m, 1H), 3.07–2.85 (m, 4H), 1.53–1.21 (m, 6H), ^{13}C NMR ($(CD_3)_2SO$, 75 MHz): δ (ppm) 172.7, 171.9, 156.0, 155.8, 143.8, 143.7, 140.6, 137.3, 129.0, 128.0, 127.5, 127.0, 126.3, 125.2, 125.0, 120.0, 65.5, 65.1, 54.4, 53.2, 48.5, 46.7, 46.6, 36.6, 31.6, 29.0, 22.7.

2.1.9. Fmoc-Lys(Fmoc)-Ala-Gly-OH (5)

Starting from Fmoc-Gly-Wang resin (300 mg, 0.18 mmol, sust.: 0.6 mmol/g) and following the general procedure I, using Fmoc-Ala-OH (168 mg, 0.54 mmol) and Fmoc-Lys-Fmoc (318 mg, 0.54 mmol), we obtained the crude material that was purified by silica gel column chromatography (CH_2Cl_2/MeOH, 95:5, drops of AcOH) providing 21.4 mg of compound **5** (20% yield).

^{1}H NMR ($(CD_3)_2SO$, 300 MHz): δ (ppm) 8.08 (m, 1H), 7.97 (m, 1H), 7.87 (m, 3H), 7.72–7.64 (m, 3H), 7.47–7.28 (m, 8H), 4.26–4.18 (m, 5H), 3.96 (m, 1H), 3.75–3.69 (m, 1H), 2.95 (m, 2H), 1.62–1.21 (m, 3H), 1.20 (d, J = 7.4 Hz, 3H). ^{13}C NMR ($(CD_3)_2SO$, 75 MHz): δ (ppm) 172.8, 172.1, 171.5, 156.5, 144.3, 144.2, 141.1, 128.0, 127.5, 125.7, 125.6, 120.5, 66.04, 65.6, 49.0, 48.3, 47.2, 47.1, 32.0, 29.5, 23.3, 18.8.

2.1.10. Fmoc-Phe-Gly-OH (6)

Starting from Fmoc-Gly-Wang resin (300 mg, 0.21 mmol, sust: 0.70 mmol/g) and following general procedure I, using Fmoc-PheOH (244 mg, 0.63 mmol), we obtained the crude material that was purified by silica gel column chromatography (CH_2Cl_2/MeOH, 95:5, drops of AcOH) providing 16.2 mg of compound **6**.

^{1}HNMR ($(CD_3)_2CO$, 300 MHz): δ (ppm) 7.39 (d, J = 7.3 Hz, 2H), 7.35–7.16 (m, 11*H*), 4.59–4.52 (m, 1H), 4.29–4.12 (m, 3H), 4.01 (d, J = 5.7 Hz, 2H), 3.27 (dd, J_1 = 14.0 Hz, J_2 = 4.2 Hz, 1H), 2.96 (dd, J_1 = 14 Hz, J_2 = 9.6 Hz, 1H); ^{13}CNMR ($(CD_3)_2CO$, 75 MHz): δ (ppm) 172.7, 172.2, 171.3, 156.8, 144.9, 142.0, 138.6, 130.2, 129.0, 128.4, 127.9, 127.2, 126.2, 126.1, 120.7, 67.2, 57.1, 47.8, 41.5, 38.8. HRMS calcd. for $C_{26}H_{23}N_2Na_2O_5^+$ $[(M-H)+2Na]^+$, *m/z*: 489.1397; found: 489.1378.

2.1.11. Fmoc-Asp-Tyr-OH (7)

Starting from Fmoc-Tyr(*t*-Bu)-Wang resin (300 mg, 0.21 mmol, sust: 0.70 mmol/g) and following general procedure I, using Fmoc-Asp (O*t*Bu)OH (300 mg, 0.63 mmol), we obtained the crude material that was purified by silica gel column chromatography (CH_2Cl_2/MeOH, 95:5, drops of AcOH) providing 16.2 mg of compound **7**.

^{1}H NMR ($(CD_3)_2CO$, 300 MHz): δ (ppm) 7.84 (d, J = 7.3 Hz, 2H), 7.69 (d, J = 7.3 Hz, 2H), 7.42–7.28 (m, 4H), 7.07 (d, J = 8.3 Hz, 2H), 6.92 (d, J = 6 Hz, 1H), 6.72 (d, J = 8.3 Hz, 2H), 4.69–4.57 (m, 2H), 4.32–4.21 (m, 3H), 3.12–2.70 (m, 5H). ^{13}C NMR ($(CD_3)_2CO$, 75 MHz): δ (ppm) 172.7, 172.5, 171.3, 157.1, 145.0, 142.0, 131.3, 128.5, 128.0, 126.2, 120.8, 116.0, 67.6, 54.5, 54.5, 52.4, 47.9, 37.1, 36.5. HRMS calcd. for $C_{28}H_{25}N_2Na_2O_8^+$ $[(M-H)+2Na]^+$, m/z: 563.1401; found: 563.1383.

2.1.12. Fmoc-Glu-Tyr-OH (8)

Starting from Fmoc-Tyr(*t*-Bu)-Wang resin (285 mg, 0.19 mmol, sust: 0.7 mmol/g) and following general procedure I, using Fmoc-Glu(O*t*Bu)-OH (270 mg, 0.57 mmol). TFA re-treatment of the raw reaction was necessary to complete removal of the *tert*-butyl group. We obtained the crude material that was purified by silica gel column chromatography (CH_2Cl_2/MeOH, 95:5, drops of AcOH) providing 66.9 mg of pure compound **8** (68% yield).

^{1}H NMR ($(CD_3)_2CO$, 300 MHz): δ (ppm) 7.83 (d, J = 7.4 Hz, 2H), 7.69 (m, 2H), 7.41–7.28 m, 4H), 7.07 (d, J = 8.3 Hz, 2H), 6.72 (d, J = 8.5 Hz, 2H), 4.68 (m, 1H), 4.33–4.20 (m, 4H), 3.14–2.94 (m, 2H), 2.43 (t, J = 7.4 Hz, 2H), 2.17–1.88 (m, 2H); ^{13}C NMR ($(CD_3)_2CO$, 75 MHz): δ (ppm) 174.3, 172.9, 172.1, 157.1, 157.0, 145.1, 144.9, 142.0, 131.2, 128.5, 128.4, 127.9, 126.2, 120.7, 116.0, 67.3, 55.4, 55.0, 54.4, 48.0, 37.1, 28.5.

2.2. Biophysical assays

All the compounds were dissolved in DMSO prior to experiments at a concentration of 200 mM. From this stock, serial dilutions, ranging from 0.75 to 200 μM were prepared. However, the final DMSO concentration in the analyzed samples was < 1%.

2.2.1. Thioflavin T fluorescence assay

Amyloid aggregation was measured by a Thioflavin-T (ThT) fluorescence assay, a common technique which allows to monitor fibril formation [27]. $A\beta_{42}$ was dissolved using a previously published solubilisation procedure using HFIP, DMSO and desalting column separation [28]. $A\beta_{42}$ concentration was adjusted to 25 μM using PBS buffer, pH 7.4 and a final concentration of 12 μM ThT in a 96-well plate. Fluorescence intensity was measured at 37 °C using an automated well-plate reader (TECAN Infinite 200 PRO) at an excitation wavelength of 450 nm and emission detection from 480 to 600 nm. Measurements were performed as independent triplicates. Recorded values were averaged and background measurements (buffer containing 12 μM ThT and compound) were subtracted. Statistical significance of the results was established by P-values using two-tailed t-tests (GraphPad Software).

2.2.2. Cytotoxicity assay

SH-SY5Y cells were grown in DMEM/F12 medium supplemented with 10% FBS, 1% penicillin/streptomycin and 1% nonessential amino acids (Gibco). Cells were seeded in a 96-well plate at 25,000 cells/well and maintained in phenol-red free DMEM/F12 (L-Glutamine, 15 mM HEPES) supplemented with 1% penicillin/streptomycin and incubated at 5% CO_2. Samples containing 25 μM $A\beta_{42}$, in absence or presence of 50 or 0.75 μM of compound **7**, were pre-incubated at r.t. for 2 h and added to the cells. As a positive control an 8% SDS solution was included. The plates were incubated at 37 °C for 48 h, followed by addition of CellTiter-Blue® Reagent (20 μL/well) and incubation for 4 h. The fluorescence intensity (excitation wavelength 560 nm and emission wavelength 590 nm) was measured using a TECAN Infinite 200 PRO fluorescence platereader. The medium background values were subtracted from the values obtained in experimental wells.

2.2.3. Transmission electron microscopy

An isoform of $A\beta_{42}$ was synthesised by Bozso et al., as described earlier [29]. The peptide was dissolved in 100 mM NaOH (pH = 11) to a concentration of 1 mg/ml. The stock solution was sonicated for 3 min then incubated for 2 h at r.t., aliquoted and snap-frozen for further use. Prior to the experiments, stock aliquots were diluted with 20 mM PBS (pH = 7.4) to a final concentration of 25 μM. To the peptide solutions, either DMSO (vehicle) or compound **7** dissolved in DMSO was added at two final concentrations, 25 μM or 100 μM. The samples were incubated for 37 °C for 0 min, 24 h and 168 h, and following incubation, 10 μL aliquots were placed on formvar carbon 400-mesh copper grids (Electron Microscopy Sciences, Washington, PA, USA). Grids were stained with 2% (w/v) uranyl acetate. Images were taken on a JEOL JEM-1400 transmission electron microscope (JEOL Ltd., Japan) operating at 120 kV. Images were captured at magnifications of x 25,000 and 40,000 and analysed with a SightX Viewer Software (EM-15300SXV Image Edit Software, JEOL Ltd., Tokyo, Japan).

2.3. Molecular modelling

PDB entry 1IYT was selected as starting monomeric conformation of $A\beta_{42}$. This conformation was determined by NMR measurements in apolar environment [30], being characterized by two helices between the 8–25 and the 28–39 residues. The starting structure was a highly helical conformation of the monomer in order to start the simulation from a close state of the cleavage, which according to the literature [31] can occur in an α-helical state of the Aβ section in the Amyloid Precursor Protein. Compound **7** was optimized first at molecular mechanical level, with PRCG (Polak-Ribiere Conjugate Gradient) method [32] using Macromodel [33] from the Schrodinger suit and it was further optimized with Gaussian09 [34] at HF/6–31 g level of theory. The atomic charges were taken from the quantum calculation and attached to the structure parameters with the Antechamber [35] program. Other force constant parameters of compound **7** were based on the GAFF parameter set [36].

2.3.1. Simulation details

Sampling conformational space of monomeric $A\beta_{42}$ in the presence and absence of compound **7**, Replica Exchange Molecular Dynamics (REMD) simulations were carried out in explicit solvent with the GROMACS 5.1 package using the AMBER99SB-ILDN force field for the $A\beta_{42}$ peptide. A dodecahedron box with 1.2 nm distance between the box and the solute was taken and solvated with explicit TIP3P water molecules. The system was neutralized with Na^+ ions and further Na^+Cl^- ion pairs were added to mimic the physiological (0.15 M) salt concentration. Both systems ($A\beta_{42}$ and $A\beta_{42}$ + ligand) were energy minimized with 50,000 steepest-descent steps. After minimization the system was heated up and 200 ps long NPT and NVT equilibrated at 315 K. For REMD simulations, 48 replicas were taken in the range of 315 K and 400 K using the temperature distribution provided by the web server of D. Van der Spoel [37]. Each replica was 250 ns long and temperature coupling was applied using velocity rescaling with a stochastic term [38] (0.1 ps time constant), as well as the isotropic Parrinello-Rahman barostat [39] with 0.5 ps time constant. P-LINCS algorithm [40] was selected for hydrogen atom connection constrains and in the electrostatic interaction the Particle Mesh Ewald (PME) method [41] was applied.

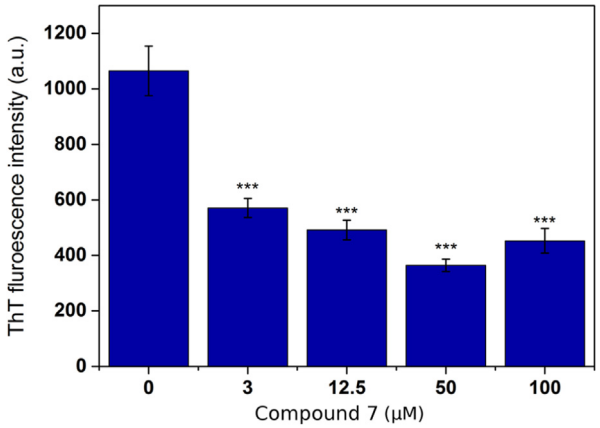

Fig. 2. $A\beta_{42}$ amyloid aggregation is affected in a dose-dependent manner by compound **7**. Dose-response amyloid fibril formation of 25 μM $A\beta_{42}$ incubated in the presence of compound at 37 °C for 7 days was monitored using ThT fluorescence intensity at 485 nm. Values represent results of three independent replicates. Statistical significance of the results was established by P-values using paired two-tailed t-tests. Statistical significance levels were * $P < 0.05$, ** $P < 0.005$ and *** $P < 0.0005$.

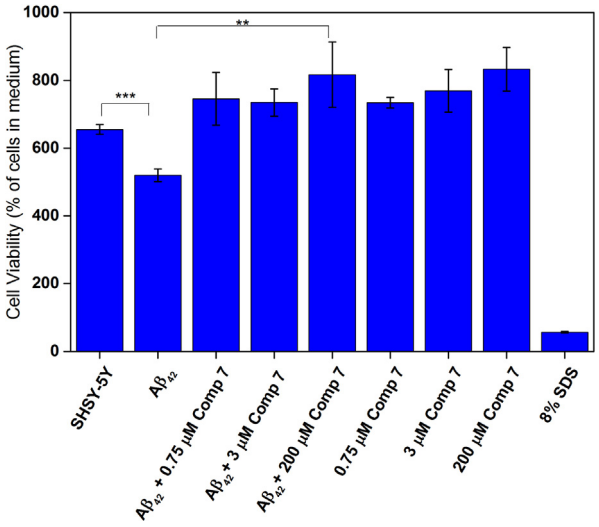

Fig. 3. Cell viability assay using the CellTiter-Blue reagent with SHSY-5Y cells exposed to 25 μM $A\beta_{42}$ in presence or absence of compound **7**. Controls include 8% μM solution of sodium dodecyl sulfate, full-length $A\beta_{42}$, compound and cells in buffer. The results are represented as mean values ± standard error of the mean. Values represent results of three independent replicates. Significant p-values are indicated by: * $P < 0.05$, ** $P < 0.01$ and *** $P < 0.001$.

2.3.2. Ensemble analysis

Two time periods were selected for analysis from the lowest temperature (315 K) replicas: the first 50 ns and the last 150 ns period. The recently published Dihedral-based Segment Identification and Classification method (DISICL) [42] was applied to calculate the secondary structure distribution for each residue. The contact maps are based on the probability of contacts over the selected periods. Two residues were considered to be in contact if their centre of mass distance is equal or lower than 0.4 nm.

2.3.3. Docking

The pure $A\beta_{42}$ monomer simulation was clustered with single linkage method taking the last 150 ns from the full trajectory. Considering clusters with more than 100 cluster members, the average middle structures were selected as representants of the trajectory for docking calculations. Compound **7** was docked onto these representants using the Glide software [43]. First, blind dockings were performed with the single precision (SP) method, where the inner box size was adjusted to 40–40–40 Angstrom (Å) while the outer box size was set to 76–76–76 Å. Refining the blind docking results, the top 5 positions were selected, and redocked using the extra precision (XP) as well as the induced fit docking (IFD) methods [44]. XP-dockings were performed with 20–20–20 and 35–35–35 Å inner and outer box size, respectively. All the other docking parameters were kept at its default values during SP or XP docking calculations, as well as the IFD using standard protocol with default settings. All interaction energies are characterized by the Glide-score values [43] which is a widely accepted scoring function for computational binding affinity prediction. The Glide score takes into account many aspects of a ligand-protein interaction just like hydrogen bonds, rotatable bond penalty, and contributions from protein-ligand coulomb-vdW energies, as well as a consequence of the hydrophobic environment.

3. Results and discussion

3.1. Searching new inhibitors preventing conformational transition of $A\beta_{42}$ monomer

In search for new inhibitors with improved potency to modulate $A\beta_{42}$ aggregation, our previously reported compound **DZK** (Fig. 1) was used as initial structure from which further optimizations were explored. The general structure of this compound consists of four parts: the core (amino acid Lys) and three substituents located at its α-carboxylic (R1), α-amine (R2) and ε-amine group (*R*3). The strategy chosen for the design of the eight new structures was based on the modification of natural amino acids with aromatic or hydrophobic substituents hypothesised to interact with the central hydrophobic cluster (CHC) of the $A\beta_{42}$ peptide. Compounds **1**, **2** and **3** presented minor variations compared to **DZK** by maintaining the Lys core and introducing new substituents in R1 = Z (compound **1**); R2 = Fmoc (compound **2**); and *R*3 = Boc (compound **3**). Compounds **4** and **5** not only presented modified substitution patterns with R2 = *R*3 = Fmoc but also extra residues at R1 like Phe (compound **4**) and Ala-Gly (compound **5**). Finally, compounds **6**, **7** and **8** presented major variations losing the characteristic Lys core. Compound **6** core was formed by the dipeptide Phe-Gly; compound **7** by Asp-Tyr; and compound **8** by Glu-Tyr. These last three structures were modified in their *N*-terminal moieties with the Fmoc group as substituent.

To evaluate the inhibition of $A\beta_{42}$ aggregation, a ThT study was performed incubating $A\beta_{42}$ peptide for seven days at 37 °C in the absence and presence of this new series of compounds. Of the eight studied mimetic peptides only compound **7** showed activity being considerably more potent at inhibiting ThT-positive $A\beta_{42}$ aggregation compared to the previously reported **DZK** (Fig. 2) [21]. Namely, DZK 100 μM was needed to reduce by 50% the ThT positive aggregates while compound **7** reached similar inhibitory activity at 3 μM concentrations.

To obtain further insight into the effect of compound **7** on the $A\beta_{42}$ aggregation kinetics a ThT assay was performed monitoring fluorescence intensity at different times of incubation. Similar to the 7-day incubation shown in Fig. 2, after 1.5 hrs ThT-positive $A\beta_{42}$ formation was diminished in a dose-dependent manner suggesting its potential interaction with $A\beta_{42}$ monomers or early aggregation species (Fig. S1, Supplementary material).

Supplementary data associated with this article can be found, in the online version, at https://doi.org/10.1016/j.bioorg.2018.08.018.

The inhibitory effect of compound **7** over $A\beta_{42}$ aggregates was further established using a cytotoxicity assay and TEM analysis. A cell viability assay, Cell Titer-Blue, demonstrated that 25 μM (based on monomeric concentration) of oligomeric $A\beta_{42}$ induced significant loss of viability in an SHSY-5Y neuroblastoma cell line. Co-incubation of 25 μM $A\beta_{42}$ oligomers with compound **7** at a concentration as low as 0.75 μM resulted in complete prevention of $A\beta_{42}$-mediated cell toxicity.

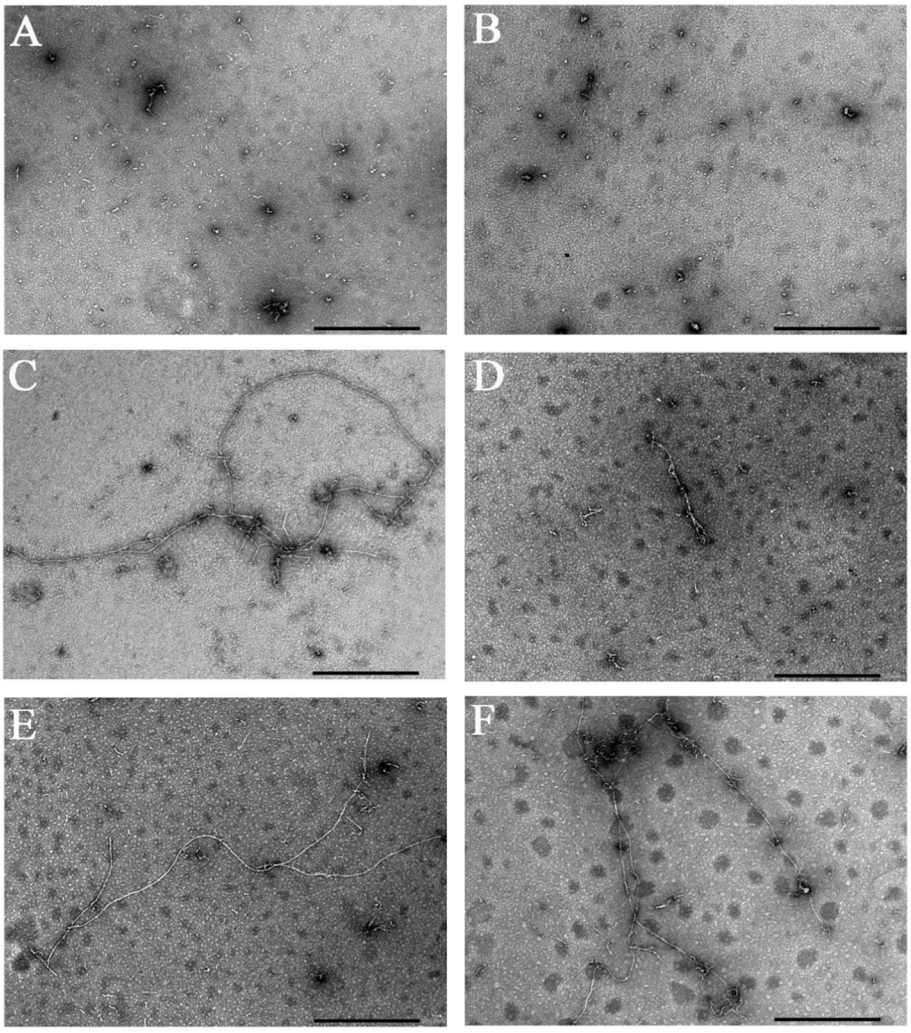

Fig. 4. Representative transmission electron microscopy images of $A\beta_{42}$ incubated either in the presence of DMSO or 25 μM compound **7**. Images were taken at three time points. 0 min: $A\beta_{42}$ with DMSO (A) or 25 μM compound **7** (B). 24 h: $A\beta_{42}$ with DMSO (C) or 25 μM compound **7** (D). 168 h: $A\beta_{42}$ with DMSO (E) or 25 μM compound **7** (F). Scale bar: 500 nm.

Moreover, the compound itself was found to be non-toxic at concentrations up to 200 μM compared to SDS 8% which was used as a control for cell death (Fig. 3).

Complementary, we conducted an *in vitro* fibril formation experiment in order to assess the effect of compound **7** on the aggregation process of $A\beta_{42}$ by TEM. Compound **7** was dissolved in DMSO and added in two different concentrations of 25 and 100 μM to a solution of 25 μM freshly-prepared $A\beta_{42}$ oligomers. The peptide solutions were incubated at 37 °C, and aliquots were analysed by TEM at three time points: 0 min, 24 h and 168 h. Fig. 4 shows representative images of the $A\beta_{42}$ oligomers incubated with a concentration of 25 μM compound **7**. Images were analysed according to the main morphological characteristics of the formed aggregates on randomly selected images (Table 1). According to the results of the analysis, average diameters of the aggregates did not change with time considerably. Lengths of fibrillary aggregates varied in a wide range, but the semi-quantitative evaluation allows a rough estimation for the size distribution. According to this, we can conclude that after 24 h, the length of the fibrils fell in a lower size range when treated with compound **7** (Fig. 4D) than without it (Fig. 4C). This difference in the lengths between the two samples was later partly equalized, as large, mature fibrils formed in both samples after 168 h. These results indicate that although compound **7** can not hinder the fibril formation, it influences the kinetics of the aggregation.

3.2. Molecular modelling

In order to have an atomistic insight into the experimentally hard to realize early stage effect of the most promising ligand, computational

Table 1
Average diameters of the aggregates and length intervals of the fibrillar forms.

	0 min		24 h		48 h	
	Diameter	Length	Diameter	Length	Diameter	Length
$A\beta_{42}$ oligomers	8.3 ± 2.4 nm	22–85 nm	7.6 ± 1.3 nm	60–842 nm	8.9 ± 1.8 nm	55–760 nm
$A\beta_{42}$ + Compound **7**	6.7 ± 1.2 nm	28–62 nm	6.8 ± 1.2 nm	29–240 nm	7.2 ± 1.9 nm	24–450 nm

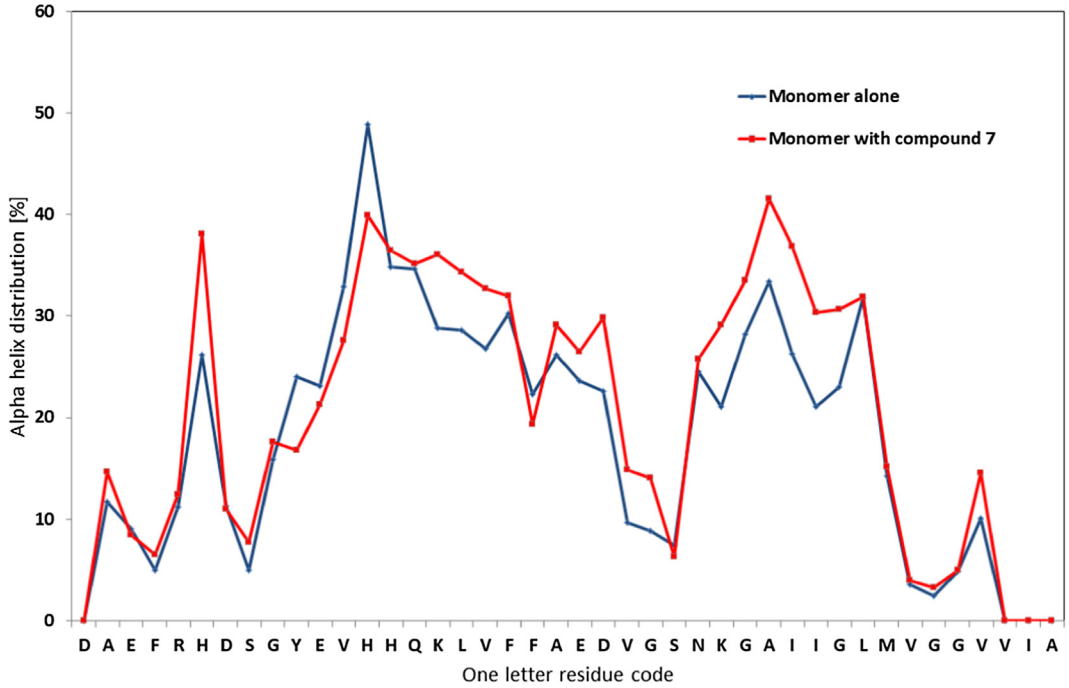

Fig. 5. The α-helical content of the $A\beta_{42}$ peptide in the presence (red) and the absence (blue) of compound **7** taking the first 50 ns of the trajectories at the lowest temperature.

investigations were carried out regarding the interaction of compound **7** and the monomeric $A\beta_{42}$. MD analysis and docking studies were applied for the computationally derived $A\beta_{42}$ peptide ensemble, which represent the conformational space immediately after the enzymatic cleavage as well as for a more general state of the $A\beta_{42}$ monomer.

Considering the MD studies, two parts of the trajectories were examined using replicas at the lowest temperature (315 K). The simulations were started from a highly helical experimental conformation of the peptide which mimicked an initial stage after cleavage and the first 50 ns were selected to see how the presence or the absence of the ligand affected the helical content. Secondly, the last 150 ns parts were considered from the same replicas to examine the effect of the ligand on the conformation space of the $A\beta_{42}$ monomer characterized by a higher disordered content.

Docking calculations followed the MD simulations and molecular targets were taken as cluster representatives of the $A\beta_{42}$ monomer derived from the last 150 ns part of the replica at the lowest temperature. These calculations allowed us to examine the ligand binding energies concerning the $A\beta_{42}$ monomer in a broader conformational scenario.

3.2.1. Maintenance of the original helical content

As was outlined in our previous articles [21,24], a possible strategy to decrease the toxicity of the $A\beta_{42}$ peptide is to avoid its transition to a β-hairpin conformation, which is related to the formation of toxic oligomers. This goal can be achieved by stabilizing the early stage conformation of the $A\beta_{42}$ monomer characterized by its high α-helical or random coiled content. Therefore, we employed the model from the PBD entry 1IYT as our starting configuration, which has been determined in an apolar environment and is characterized by two α-helical regions (residues 8–25 and 28–39). Considering the first 50 ns from the REMD simulations we found that compound **7** inhibited the loss of helical structure especially on the C-terminal region compared to the pure $A\beta_{42}$ monomer simulation (see Fig. 5).

To elucidate the contact between the protein and the ligand we calculated their centre of mass distances (the resulting contact distribution is shown in Fig. S2, Supplementary material). It was found that the largest number of contacts between the ligand and the monomer peptide was found within the helical regions in particular the one comprised between the residues 16 and 20. As Fig. 5 presents, the helical content also increased partly in this region between $K^{16}LV^{18}$ residues. It is worth to note that the hydrophobic interaction between the β-strand $K^{16}LVFFA^{21}$ and $N^{27}KGAIIG^{33}$ regions has important role in the formation of the β-hairpin conformation.

3.2.2. Secondary structure elements progression

To have a general picture about the effect of compound **7** to the monomeric state of $A\beta_{42}$ peptide, we compared secondary structure elements between the ligand + monomer and the free monomer cases using the last 150 ns of the replicas with the lowest temperature. Difference between the probability of α-helix (red), 3_{10}-helix (blue) and β-strand (green) for each residue is presented in Fig. 6.

We found that in the presence of compound **7** the β-strand content was significantly diminished at $K^{16}LVFFA^{21}$ (CHC), $S^{26}N^{27}$ and $A^{30}II^{32}$ segments. These residues are mainly involved in the formation of hairpin structures in the $A\beta_{42}$ toxic aggregates [45,46]. This difference observed with the free ligand system had as counterpart increased 3_{10}-helix propensities between $S^{8}GYEYH^{13}$ and CHC region. We also observed higher α-helical distribution between $N^{27}KGAIIG^{33}$ residues. These results are consistent with theoretical [47] and experimental [48] studies which posit that the preservation of these helical regions can stop oligomerization at the dimer stage by impeding unfolding and β-sheet formation.

3.2.3. Contacts between $A\beta_{42}$ monomer and compound 7 during REMD simulations

Following the original principle of the design we dissect compound **7** into three fragments namely Fmoc, Asp and Tyr-OH. These segments presented different interactions with the $A\beta_{42}$ monomer *i.e.* hydrophobic (Fmoc, Tyr-OH), ionic (Asp) or hydrogen-bond (Tyr-OH, peptide-bonds). Then, we calculated the centre of mass distances between each residues of the protein and the three fragments, where the critical distance for a contact was defined as less than or equal to 0.4 nm. Fig. 7 shows the contact distribution per residue between the $A\beta_{42}$ monomer and the three major parts of the ligand. The highly aromatic Fmoc

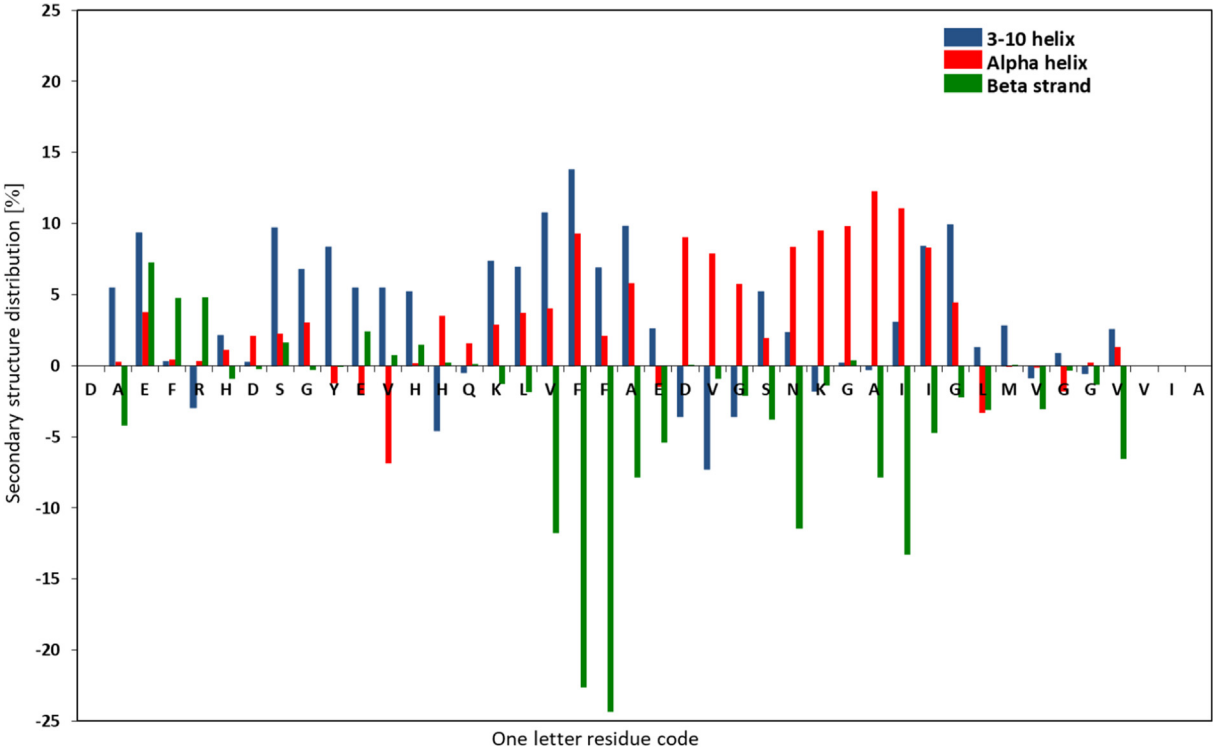

Fig. 6. Difference between the probability of secondary structure elements adopted by the $A\beta_{42}$ peptide in the presence and absence of compound **7** taking the last 150 ns of the trajectories at the lowest temperature. Colour code: α-helix (red), 3_{10}-helix (blue) and β-strand (green).

group often forms contacts with residues 12–19 and 28–38 providing a putative explanation for the inhibitory capacity of compound **7** on the conformational transition of the $A\beta_{42}$ monomer.

3.2.4. Estimating potential binding modes

To have a more depicted description of putative binding modes between compound **7** and the $A\beta_{42}$ monomer different docking calculations were performed. Here, we considered the dynamical character of the peptide by generating multiple docking targets. The targets were derived by clusterization of the last 150 ns of the lowest temperature $A\beta_{42}$ monomer trajectory taken from the previous REMD study. According to this, 4602 clusters were generated, of which only the ones with more than 100 elements were selected. This way 21 clusters representants were selected to perform blind docking with the quickest SP method. The best docking scores of each target are reported in Table S1 (Supplementary material).

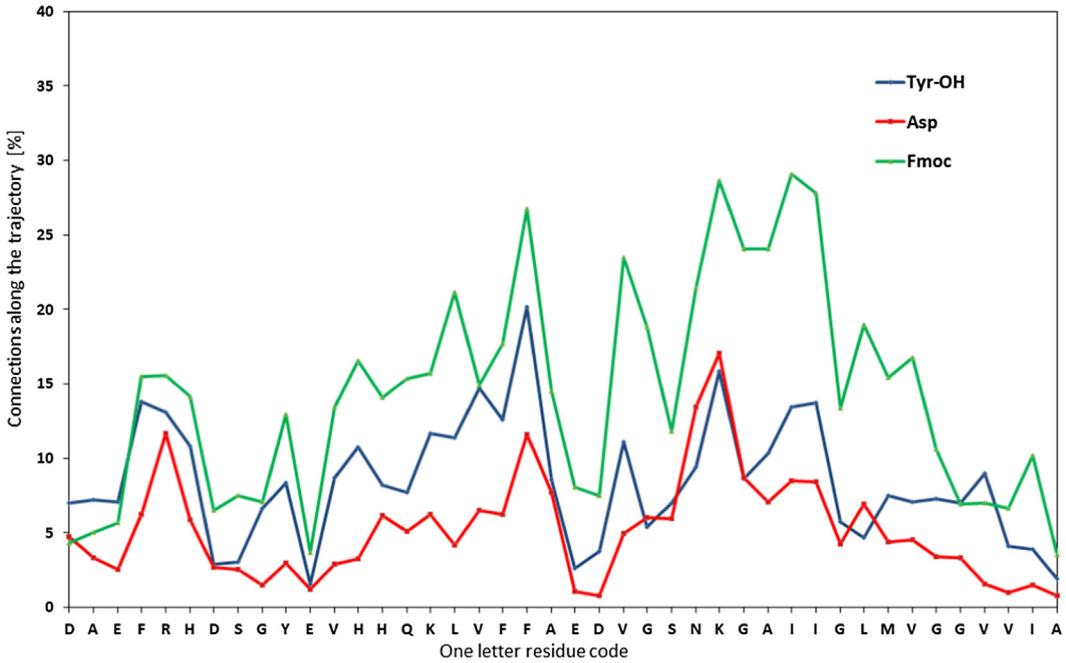

Fig. 7. Distribution of the contacts between compound **7** and the $A\beta_{42}$ monomer in the last 150 ns of the trajectory taking the lowest temperature.

Table 2
Single precision, extra precision and induced fit docking scores.

	Docking method		
Cluster	Single precision	Extra precision	Induced fit docking
787	−6.422	−3.48	−9.60
1415	−6.399	−3.54	−7.47
3691	−6.115	−6.82	−8.32
1954	−5.566	−6.14	−6.50
3354	−5.367	−5.89	−8.35

To refine our blind docking results, we selected 5 complexes with the best SP docking values and performed XP and IFD calculations. Refining docking was restricted to a 20 Å environment of the poses provided by the blind docking SP calculations. All Glide score values (SP, XP and IFD) are shown in Table 2. As can be observed, score rankings were not maintained when using the different docking approaches.

Nevertheless, the analysis of the highest and lowest binding energies provided hints about relevant interactions between compound **7** and the $A\beta_{42}$ monomer. For example, in the case of cluster 787 both SP and IFD showed the higher scorings among the five analysed systems while XP method presented the weakest interaction with the peptide. This main difference could be explained considering how in the first two methods compound **7** formed π-stacking interactions between the Fmoc group and aromatic residues His^{14} and Tyr^{10} (SP and IFD methods, respectively) while in the XP case this interaction was lost leaving the hydrophobic group exposed to the solvent and so reducing its binding affinity to the $A\beta_{42}$ peptide. Other preferred binding modes, *e.g.* the one obtained in cluster 3354 using the IFD method showed the same peculiarity having π-stacking interactions with Tyr^{10}. Another important feature in this particular binding mode were two salt-bridges formed between Lys^{28} and Arg^{5} with the COO^- groups of **7** (Fig. 8).

Overall, the close interaction of compound **7** burying its hydrophobic group in the CHC of $A\beta_{42}$ regardless of the peptide conformation coincides with the results observed in the REMD trajectory where the contact distribution of the ligand was located in this region of the $A\beta_{42}$ monomer. This interaction is in line with the capacity of the ligand to inhibit the conformational transition in the $L^{17}VFFA^{21}$ region towards higher contents of β-strand structures.

4. Conclusions

In a previous work we reported a mimetic peptide, **DZK**, possessing a potent inhibitory effect on $A\beta_{42}$ aggregate formations [21]. Here, we investigated experimentally a new series of mimetic peptides based on the **DZK** molecule completed with detailed theoretical analysis for a selected case. Among the tested molecules, compound **7** possessed a higher inhibitory potency at ThT-positive $A\beta_{42}$ aggregation than the original **DZK** molecule. This compound was selected for a more extensive physico-chemical evaluation including a ThT assay monitoring fluorescence intensity at different times and TEM studies, as well as a cell viability assay to obtain further insights into the prevention of $A\beta_{42}$ -mediated cell toxicity.

Moreover, different computational modelling techniques were employed to identify the interactions of compound **7** with early stage $A\beta_{42}$

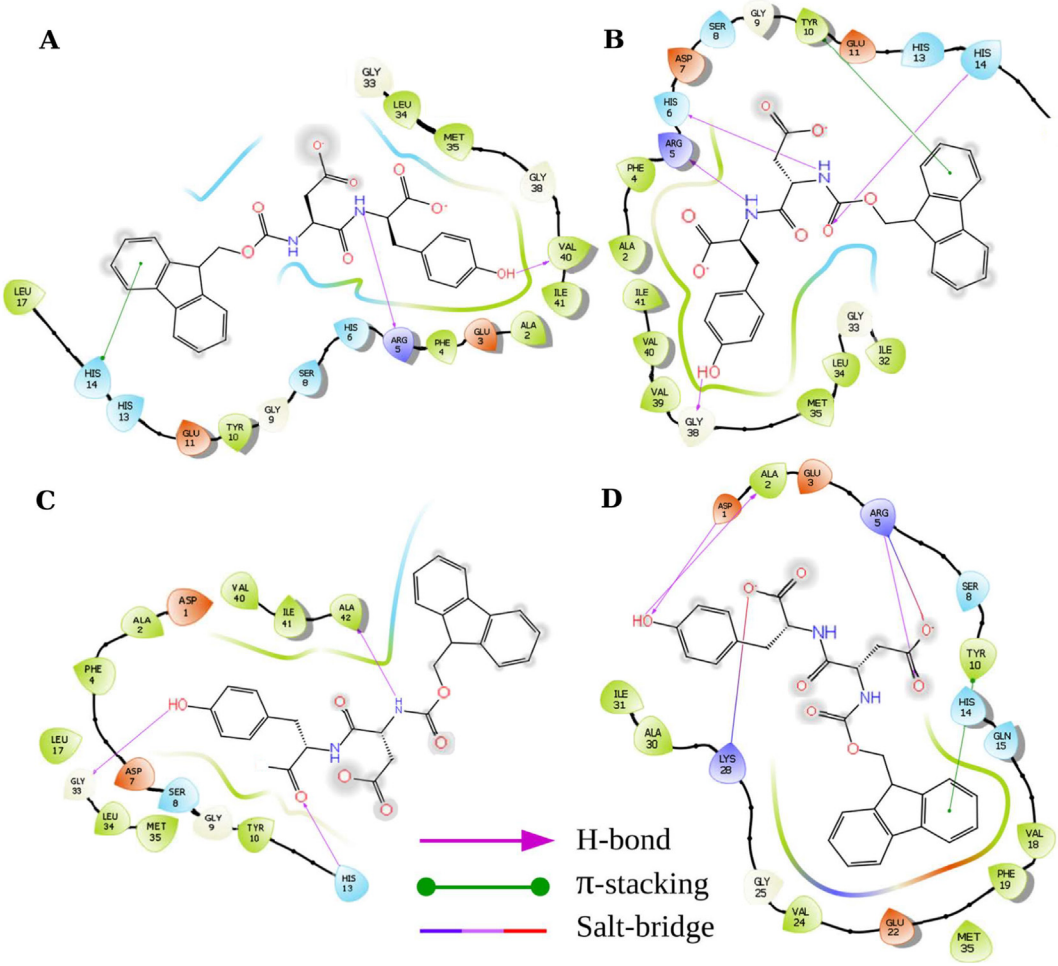

Fig. 8. 2-D diagrams of **7**-$A\beta_{42}$ complexes for cluster 787 employing different docking methods: SP (A), IFD (B), XP (C) and cluster 3354 employing IFD (D).

monomer and look for possible explanations of how this mimetic peptide affects the conformational transition of the peptide. These simulations enabled us to obtain a picture for the experimentally hard to attain, very early stage interaction with the ligand at atomic level. REMD simulations showed that compound **7** diminished the formation of aggregation-prone structures by maintaining helical content which were reproduced by our ligand-free control simulations. It was also found that the β-strand structure was significantly diminished at CHC region (residues $K^{16}LVFFA^{21}$). Regarding helical structures, the α-helical distribution was higher at $N^{27}KGAIIG^{33}$ residues and 3_{10}-helix propensities were increased at *N*-terminal and CHC regions in the presence of compound **7**. These secondary structure results are in good agreement with experimental [46] and theoretical [47] studies where it had been indicated that the loss of helical content can be observed during the early stage of toxic species formation.

Molecular docking studies revealed that compound **7** interacted with the $A\beta_{42}$ monomer through π-stacking interactions between its Fmoc group and the aromatic residues His^{14} or Tyr^{10}. Compound **7** buries its hydrophobic Fmoc group in the CHC leading to the dominance of helical conformation in this region. This result corroborates the REMD simulations where the contact distribution of the ligand is also enhanced at the CHC region of the $A\beta_{42}$ monomer.

In conclusion, our experimental and theoretical work demonstrated that compound **7** modulates the early steps of the amyloidogenic process also inhibiting the cytotoxicity linked to $A\beta_{42}$ aggregation with full viability recovery of cultured cells under submicromolar concentrations of the ligand.

Acknowledgments

Grants from Universidad Nacional de San Luis (UNSL), partially supported this work. This research was also supported by Agencia Nacional de Promoción Científica y Tecnológica (PICT 2015-1769). L.M.; C.M.L.D and E.G.M. thank CONICET, ANPCyT and UNR for support. E.E.B. is beneficiary of a postdoctoral fellowship of CONICET (Consejo Nacional de Investigaciones Científicas y Técnicas, Argentina). Some of the authors (J.G., T.Sz., L.F. and G.P.) acknowledge financial support from the Hungarian government (GINOP-2.3.2-15-2016-00034) and from the Hungarian Scientific Research Fund (OTKA) K111862.

References

[1] I. Melnikova, Therapies for Alzheimer's disease, Nat. Rev. Drug Discov. 6 (2007) 341–352.
[2] H.W. Querfurth, F.M. LaFerla, Alzheimer's disease, N. Engl. J. Med. 362 (2010) 329–344.
[3] 2012 Alzheimer's disease facts and figures, Alzheimer's Dement. 8 (2012) 131-168.
[4] J. Hardy, D.J. Selkoe, The amyloid hypothesis of Alzheimer's disease: progress and problems on the road to therapeutics, Science 297 (2002) 353–356.
[5] A.S. Cohen, L.A. Jones, Amyloid and amyloidosis, Curr. Opin. Rheumatol. 3 (1991) 125–138.
[6] M.A. Findeis, The role of amyloid beta peptide 42 in Alzheimer's disease, Pharmacol. Ther. 116 (2007) 266–286.
[7] D.M. Walsh, D.J. Selkoe, Aβ oligomers – a decade of discovery, J. Neurochem. 101 (2007) 1172–1184.
[8] E. Hayden, D. Teplow, Amyloid β-protein oligomers and Alzheimer's disease, Alzheimer's Res. Ther. 5 (2013) 60.
[9] J.E. Gestwicki, G.R. Crabtree, I.A. Graef, Harnessing chaperons to generate small-molecule inhibitors of amyloid β aggregation, Science 306 (2004) 865–869.
[10] A.J. Doig, Peptide inhibitors of β-amyloid aggregation, Curr. Opin. Drug Discov. Dev. 10 (2007) 533–539.
[11] C. Yang, X. Zhu, J. Li, R. Shi, Exploration of the mechanism for LPFFD inhibiting the formation of β-sheet conformation of Aβ(1–42) in water, J. Mol. Model. 16 (2010) 813–821.
[12] Y. Cote, G.G. Maisuradze, P. Delarue, H.A. Scheraga, P. Senet, New insights into protein (Un)folding dynamics, J. Phys. Chem. Lett. 6 (2015) 1082–1086.
[13] R.P. Bywater, Protein folding: A problem with multiple solutions, J. Biomol. Struct. Dyn. 31 (2013) 351–362.
[14] D. Goyal, S. Shuaib, S. Mann, B. Goyal, Rationally designed peptides and peptidomimetics as inhibitors of amyloid-β (Aβ) aggregation: potential therapeutics of Alzheimer's disease, ACS Comb. Sci. 19 (2017) 55–80.
[15] D. Galimberti, E. Scarpini, Emerging amyloid disease-modifying drugs for Alzheimer's disease, Expert Opin. Emerg. Drugs 21 (2016) 5–7.
[16] Z.-L. Zhou, Y. Ho, H.-L. Liu, P. Elumalai, W.-H. Chen, Computer-aided discovery of novel non-peptide inhibitors against amyloid-beta (Aβ) peptide aggregation for treating Alzheimer's disease, Mol. Simul. 41 (2015) 622–632.
[17] L. Bellucci, A. Ardèvol, M. Parrinello, H. Lutz, H. Lu, T. Weidner, S. Corni, The interaction with gold suppresses fiber-like conformations of the amyloid β(16–22) peptide, Nanoscale 8 (2016) 8737–8748.
[18] G.S. da Silva, M. Figueiró, C.F. Tormena, F. Coelho, W.P. Almeida, Effects of novel acylhydrazones derived from 4-quinolone on the acetylcholinesterase activity and Aβ42 peptide fibrils formation, J. Enzyme Inhib. Med. Chem. 1 (2016) 1–7.
[19] W. Xu, X.-B. Wang, Z.-M. Wang, J.J. Wu, F. Li, J. Wang, L.-Y. Kong, Synthesis and evaluation of donepezil–ferulic acid hybrids as multi-target-directed ligands against Alzheimer's disease, Med. Chem. Commun. 7 (2016) 990–998.
[20] J. Nasica-Labouze, P.H. Nguyen, F. Sterpone, O. Berthoumieu, N. Buchete, S. Coté, A. De Simone, A.J. Doig, P. Faller, A. Garcia, A. Laio, M. Suan Li, S. Melchionna, N. Mousseau, Y. Mu, A. Paravastu, S. Pasquali, D.J. Rosenman, B. Strodel, B. Tarus, J.H. Viles, T. Zhang, C. Wang, P. Derreumaux, Amyloid β protein and Alzheimer's disease: when computer simulations complement experimental studies, Chem. Rev. 115 (2015) 3518–3563.
[21] E.E. Barrera Guisasola, S.A. Andujar, E. Hubin, K. Broersen, I.M. Kraan, L. Méndez, C.M.L. Delpiccolo, M.F. Masman, A.M. Rodríguez, R.D. Enriz, New mimetic peptides inhibitors of Aβ aggregation. Molecular guidance for rational drug design, Eur. J. Med. Chem. 95 (2015) 136–152.
[22] E.E. Barrera Guisasola, L.J. Gutierrez, S.A. Andujar, E. Angelina, A.M. Rodríguez, R.D. Enriz, Pentameric models as alternative molecular targets for the design of new antiaggregant agents, Curr. Prot. Pept. Sci. 17 (2016) 156–168.
[23] M.F. Masman, U.L.M. Eisel, I.G. Csizmadia, B. Penke, R.D. Enriz, S.J. Marrink, P.G.M. Luiten, In silico study of full-length amyloid 1–42 tri- and penta-oligomers in solution, J. Phys. Chem. B. 113 (2009) 11710–11719.
[24] E.E. Barrera Guisasola, L.J. Gutiérrez, R.E. Salcedo, F.M. Garibotto, S.A. Andujar, R.D. Enriz, A.M. Rodríguez, Conformational transition of Aβ42 inhibited by a mimetic peptide. A molecular modeling study using QM/MM calculations and QTAIM analysis, Comput. Theor. Chem. 1080 (2016) 56–65.
[25] F. Albericio, Solid-phase Synthesis: A Practical Guide, CRC Press, 2000.
[26] N.L. Benoiton, Chemistry of Peptide Synthesis, Taylor & Francis, London, 2005.
[27] M. Biancalana, S. Koide, Molecular mechanism of thioflavin-T binding to amyloid fibrils, Biochim. Biophys. Acta 1804 (2010) 1405–1412.
[28] K. Broersen, W. Jonckheere, J. Rozenski, A. Vandersteen, K. Pauwels, A. Pastore, F. Rousseau, J. Schymkowitz, A standardized and biocompatible preparation of aggregate-free amyloid beta peptide for biophysical and biological studies of Alzheimer's disease, Prot. Eng. Des. Sel. 9 (2011) 743–750.
[29] Z. Bozso, B. Penke, D. Simon, I. Laczko, G. Juhasz, V. Szegedi, A. Kasza, K. Soos, A. Hetenyi, E. Weber, H. Tohati, M. Csete, M. Zarandi, L. Fulop, Controlled in situ preparation of A beta(1–42) oligomers from the isopeptide "iso-A beta(1–42)", physicochemical and biological characterization, Peptides 31 (2010) 248–256.
[30] O. Crescenzi, S. Tomaselli, R. Guerrini, S. Salvadori, A.M. D'Ursi, P.A. Temussi, D. Picone, Solution structure of the Alzheimer amyloid β-peptide (1–42) in an apolar microenvironment, Eur. J. Biochem. 269 (2002) 5642–5648.
[31] S.S. Sisodia, Beta-amyloid precursor protein cleavage by a membrane-bound protease, PNAS 89 (1992) 6075–6079.
[32] E. Polak, G. Ribiere, Note sur la Convergence de Methods de Directions Conjugres, Revue Francaise Informat. Recherche Operationnelle 16 (1969) 35–43.
[33] 2017-3, S. R. MacroModel, New York, 2017.
[34] M.J. Frisch, G.W. Trucks, H.B. Schlegel, G.E. Scuseria, M.A. Robb, J.R. Cheeseman, G. Scalmani, V. Barone, G.A. Petersson, H. Nakatsuji, X. Li, M. Caricato, A. Marenich, J. Bloino, B.G. Janesko, R. Gomperts, B. Mennucci, H.P. Hratchian, J.V. Ortiz, A.F. Izmaylov, J.L. Sonnenberg, D. Williams-Young, F. Ding, F. Lipparini, F. Egidi, J. Goings, B. Peng, A. Petrone, T. Henderson, D. Ranasinghe, V.G. Zakrzewski, J. Gao, N. Rega, G. Zheng, W. Liang, M. Hada, M. Ehara, K. Toyota, R. Fukuda, J. Hasegawa, M. Ishida, T. Nakajima, Y. Honda, O. Kitao, H. Nakai, T. Vreven, K. Throssell, J.A. Montgomery Jr., J.E. Peralta, F. Ogliaro, M. Bearpark, J.J. Heyd, E. Brothers, K.N. Kudin, V.N. Staroverov, T. Keith, R. Kobayashi, J. Normand, K. Raghavachari, A. Rendell, J.C. Burant, S.S. Iyengar, J. Tomasi, M. Cossi, J.M. Millam, M. Klene, C. Adamo, R. Cammi, J.W. Ochterski, R.L. Martin, K. Morokuma, O. Farkas, J.B. Foresman, D.J. Fox, Gaussian 09, Revision A.02, Gaussian, Inc., Wallingford CT, 2016.
[35] J. Wang, W. Wang, P.A. Kollman, D.A. Case, Automatic atom type and bond type perception in molecular mechanical calculations, J. Mol. Graph. Model. 25 (2006) 247–260.
[36] J. Wang, R.M. Wolf, J.W. Caldwell, P.A. Kollman, D.A. Case, Development and testing of a general amber force field, J. Computat. Chem. 25 (2004) 1157–1174.
[37] A. Patriksson, D. van der Spoel, A temperature predictor for parallel tempering simulations, Phys. Chem. Chem. Phys. 10 (2008) 2073–2077.
[38] G. Bussi, M. Parrinello, Accurate sampling using Langevin dynamics, Phys. Rev. E 75 (2007) 056707.
[39] M. Parrinello, A. Rahman, Polymorphic transitions in single crystals: A new molecular dynamics method, J. Appl. Phys. 52 (1981) 7182–7190.
[40] B. Hess, P-LINCS: A parallel linear constraint solver for molecular simulation, J. Chem. Theory Comput. 4 (2008) 116–122.
[41] T. Darden, D. York, L. Pedersen, Particle mesh Ewald: An N·log(N) method for Ewald sums in large systems, J. Chem. Phys. 98 (1993) 10089–10092.
[42] G. Nagy, C. Oostenbrink, Dihedral-based segment identification and classification of biopolymers I: Proteins, J. Chem. Inf. Model. 54 (2014) 266–277.
[43] R.A. Friesner, R.B. Murphy, M.P. Repasky, L.L. Frye, J.R. Greenwood, T.A. Halgren, P.C. Sanschagrin, D.T. Mainz, Extra precision glide: docking and scoring

incorporating a model of hydrophobic enclosure for protein−ligand complexes, J. Med. Chem. 49 (2006) 6177–6196.
[44] R. Farid, T. Day, R.A. Friesner, R.A. Pearlstein, New insights about HERG blockade obtained from protein modeling, potential energy mapping, and docking studies, Bioorg. Med. Chem. 14 (2006) 3160–3173.
[45] W.P. Esler, E.R. Stimson, J.R. Ghilardi, Y.A. Lu, A.M. Felix, H.V. Vinters, P.W. Mantyh, J.P. Lee, J.E. Maggio, Point substitution in the central hydrophobic cluster of a human beta-amyloid congener disrupts peptide folding and abolishes plaque competence, Biochemistry 35 (1996) 13914–13921.
[46] N.S. de Groot, F.X. Aviles, J. Vendrell, S. Ventura, Mutagenesis of the central hydrophobic cluster in Abeta42 Alzheimer's peptide. Side-chain properties correlate with aggregation propensities, FEBS J. 273 (2006) 658–668.
[47] A.V. Rojas, A. Liwo, H.A. Scheraga, A study of the α-helical intermediate preceding the aggregation of the amino-terminal fragment of the β amyloid peptide (Aβ(1–28)), J. Phys. Chem. B 115 (2011) 12978–12983.
[48] A. Kapurniotu, A. Buck, M. Weber, A. Schmauder, T. Hirsch, J. Bernhagen, M. Tatarek-Nossol, Conformational restriction via cyclization in β-amyloid peptide Aβ(1–28) leads to an inhibitor of Aβ(1–28) amyloidogenesis and cytotoxicity, Chem. Biol. 10 (2003) 149–159.